

PCCP

Accepted Manuscript



This is an *Accepted Manuscript*, which has been through the Royal Society of Chemistry peer review process and has been accepted for publication.

Accepted Manuscripts are published online shortly after acceptance, before technical editing, formatting and proof reading. Using this free service, authors can make their results available to the community, in citable form, before we publish the edited article. We will replace this *Accepted Manuscript* with the edited and formatted *Advance Article* as soon as it is available.

You can find more information about *Accepted Manuscripts* in the [Information for Authors](#).

Please note that technical editing may introduce minor changes to the text and/or graphics, which may alter content. The journal's standard [Terms & Conditions](#) and the [Ethical guidelines](#) still apply. In no event shall the Royal Society of Chemistry be held responsible for any errors or omissions in this *Accepted Manuscript* or any consequences arising from the use of any information it contains.

Dielectric spectra of ionic liquids and their conversion to solvation dynamics: A detailed computational analysis of polarizable systems

Michael Schmollngruber, Christian Schröder,^{a)} and Othmar Steinhauser

University of Vienna, Department of Computational Biological Chemistry, Währingerstrasse 17, A-1090 Vienna, Austria

(Dated: 4 April 2014)

For the three molecular ionic liquids 1-ethyl-3-methylimidazolium tetrafluoroborate, 1-ethyl-3-methylimidazolium trifluoromethanesulfonate and 1-butyl-3-methylimidazolium tetrafluoroborate, dielectric spectra were calculated from molecular dynamics simulations based on polarizable force fields. Using the reaction field continuum model the dielectric spectra were converted to the solvation dynamics of Coumarin 153. It is shown in detail that the inclusion of the static conductivity in this model is essential. When simplifying the dielectric spectrum to the static conductivity hyperbola, the solvation response function becomes mono-exponential. Taking into account the frequency dependence of the conductivity, the typical two time-regimes of the solvation response function in ionic liquids are already obtained. However, the mean relaxation time remains the same. When converting the complete dielectric spectrum, i.e. also including frequency-dependent dielectric permittivity, quantitative changes are observed, but the qualitative shape is conserved. In accordance with previous experimental studies, solvation dynamics in ionic liquids predicted by the reaction field continuum model is too fast for longer times. This correlates with the suppression of the fine structure of the dielectric spectrum at low frequencies by the static conductivity hyperbola. By scaling down the static conductivity this effect can be partially amended. In addition to the impact of the solvent dielectric spectrum on solvation dynamics, also solute-specific effects, i.e. anisotropy in shape and charge distribution as well as polarizability, were studied.

I. INTRODUCTION

Ionic liquids are characterized by an anisotropy in charge distribution and shape. This combination makes them a challenging class of soft matter when dealing with their electrostatic or dielectric properties, as they unite the properties of polar liquids and ionic melts. At the molecular level, they have a net charge and a dipole moment and as opposed to ionic solutions, both reside on the very same molecule. At the dielectric or mesoscopic level these properties correspond to the dielectric conductivity $\vartheta(\omega)$ and the dielectric permittivity $\epsilon(\omega)$, respectively.¹⁻³ While the former stands for collective translation, the latter is representative of collective rotation. In any case, it is the response to an applied external electric field, as measured in dielectric spectroscopy. An alternative method is to detect the internal Maxwell field exerted on a solute used as a probe, being Coumarin 153 in most cases.⁴⁻¹⁰ In this case, the solute is excited to its electronic S_1 state and it is the accompanying change in the dipole moment that is coupling to the Maxwell field. The relaxation of the surrounding solvent after the excitation of the solute is recorded via time-resolved fluorescence spectroscopy, yielding what is commonly known as the solvation response function or solvation dynamics. This method has a long tradition for polar solvents¹¹⁻¹⁷. In recent years, it was also applied to ionic liquids.^{5-9,18-34}

As both methods, dielectric spectroscopy and solvation

dynamics, operate with electric fields, either as a perturbation or as a response, investigations into their mutual relation exist in the literature. In most of these studies the focus was on experimental data.^{6-9,21,32,35} In this study we operate with computational methods, calculating the dielectric spectrum and the solvation response function from the very same simulation. For the conversion of the former into the latter we use the reaction field continuum model (RFCM), because it does not need data from another source than the dielectric spectrum. In previous studies based on experimental dielectric spectra, the RFCM worked very well for polar liquids, but faced problems for charged dipolar systems, i.e. ionic liquids. A computational approach allows to study how parts of the dielectric spectrum - when considered separately - influence the solvation response function. In this way we hope to elucidate the peculiar problems encountered^{6-9,32} when applying the RFCM to ionic liquids.

Recently, there have also been other attempts beyond those based on a simple continuum model to predict the solvation response function of ionic liquids, either employing a semi-molecular approach^{30,31} or an extended Debye-Hückel model⁵.

This paper is organized as follows: In the theory section a short overview of the development of the RFCM and its application to ionic liquids is given. Special attention was paid to anisotropic features of the solute C153. The results and discussion section starts with the presentation of the computational dielectric spectra. Subsequently, the solvation response function is characterized within the framework of the RFCM. Fundamental analytic results are collected in the appendix and background

^{a)}Electronic mail: christian.schroeder@univie.ac.at

information concerning the calculation of the dielectric spectra is given in the supplementary material.

II. THEORY

A. Calculation of the solvation response function from the frequency-dependent generalized dielectric constant

The normalized time-dependent solvation response function is given by

$$S(t) = \frac{\Delta U(t) - \Delta U(\infty)}{\Delta U(0) - \Delta U(\infty)}, \quad (1)$$

where $U(t)$ is the solvation energy. At time $t = 0$ the charge distribution of a chromophore molecule embedded in a solvent is changed due to photoexcitation. The relaxation of the solvent molecules in response to this change of the charge distribution $\Delta\rho(\vec{r}, t)$ of the solute results in a transient shift of the solvation energy

$$\Delta U(t) = \frac{1}{2} \int \Delta\rho(\vec{r}, t) \Phi(\vec{r}, t) d\vec{r}, \quad (2)$$

where $\Phi(\vec{r}, t)$ is the total electrostatic potential exerted by the solvent. A first approximation of this potential is given by enclosing the charge distribution of the solute $\Delta\rho(\vec{r}, t)$ in a spherical cavity of radius a and describing the solvent outside by a dielectric continuum with a static dielectric constant ϵ :

$$\Phi(\vec{r}) = \sum_{l=0}^{\infty} \sum_{m=-l}^{+l} -\frac{\epsilon - \epsilon_c}{\epsilon + \epsilon_c} \frac{1}{l+1} \frac{q_m^l}{a^{2l+1}} r^l Y_m^l(\theta, \phi). \quad (3)$$

Furthermore, it is assumed that the cavity is filled with a dielectric medium characterized by the constant ϵ_c . The spatial variation of the potential within the cavity is described by the solid spherical harmonics $r^l Y_m^l(\theta, \phi)$. The anisotropy of the charge distribution of the solute is characterized by its multipole moments

$$q_m^l = \int \Delta\rho(\vec{r}) r^l Y_m^l(\theta, \phi) d\vec{r}. \quad (4)$$

Inserting the static potential $\Phi(\vec{r})$ into Eq. 2 one gets the temporal average of the solvation energy

$$\langle \Delta U \rangle = -\frac{1}{2} \sum_{l=0}^{\infty} \frac{\epsilon - \epsilon_c}{\epsilon + \epsilon_c} \frac{1}{l+1} \frac{1}{a^{2l+1}} \sum_{m=-l}^{+l} q_m^l q_m^{l*}. \quad (5)$$

For the special case $l = 1$, i.e. for a single dipole $\vec{\mu}$ enclosed in the cavity this reduces to the original formula of Boettcher and Bordewijk³⁶

$$\langle \Delta U_{\mu} \rangle = -\frac{1}{2} \frac{\Delta\vec{\mu}^2}{a^3} \frac{\epsilon - \epsilon_c}{\epsilon + \frac{\epsilon_c}{2}} = -\frac{1}{2} \Delta\vec{\mu} \cdot \vec{E}_{RF}, \quad (6)$$

where in the second step we have introduced the reaction field

$$\vec{E}_{RF} = \frac{\Delta\vec{\mu}}{a^3} \frac{\epsilon - \epsilon_c}{\epsilon + \frac{\epsilon_c}{2}}. \quad (7)$$

The factor $\Delta\vec{\mu}^2/a^3$ in Eq. 6 is a dipolar energy representative of the solute. The dimensionless co-factor involving the dielectric constant stands for the solvation properties of the solvent. Maroncelli and Fleming³⁷ realized that Eq. 7 gives an incorrect limit for $\epsilon = 1$, i.e. the reaction field does not vanish in the absence of a solvent, but gives a value dependent on ϵ_c . In fact, this represents a spurious self-interaction of the solute dipole with its own cavity. This can be amended by the method of Mazurenko³⁸ as recommended by Maroncelli and Fleming.³⁷ This method augments the permanent dipole moment $\Delta\vec{\mu}$ by an induced contribution $\Delta\vec{\mu}_{ind} = \alpha \vec{E}_{RF}$

$$\vec{E}_{RF} = \frac{\Delta\vec{\mu} + \alpha \vec{E}_{RF}}{a^3} \frac{\epsilon - 1}{\epsilon + \frac{1}{2}}, \quad (8)$$

where α is the molecular polarizability of the solute. Consequently, ϵ_c was set to unity. However, it re-enters via the Clausius-Mosotti equation

$$\frac{\alpha}{a^3} = \frac{\epsilon_c - 1}{\epsilon_c + 2}, \quad (9)$$

yielding

$$\vec{E}_{RF} = \frac{\Delta\vec{\mu}}{a^3} \frac{\epsilon_c + 2}{3} \frac{\epsilon - 1}{\epsilon + \frac{\epsilon_c}{2}}. \quad (10)$$

So far, the reaction field is only a temporal average as it includes only the static dielectric constant. To introduce the time dependence we start from the constitutive relation in the frequency domain

$$\vec{P}(\vec{r}, \omega) = \frac{\epsilon(\omega) - 1}{4\pi} \vec{E}(\vec{r}, \omega), \quad (11)$$

giving the dielectric polarization $\vec{P}(\vec{r}, \omega)$ for systems composed of neutral dipolar molecules. Both, $\vec{P}(\vec{r}, \omega)$ and $\vec{E}(\vec{r}, \omega)$ can be combined to the dielectric displacement

$$\vec{D}(\vec{r}, \omega) = \vec{E}(\vec{r}, \omega) + 4\pi \vec{P}(\vec{r}, \omega) = \epsilon(\omega) \vec{E}(\vec{r}, \omega). \quad (12)$$

The static reaction field (Eq. 7) was obtained as a solution of the Laplace equation under the boundary conditions that the parallel component of $\vec{E}(\vec{r})$ and the normal component of $\vec{D}(\vec{r})$ are continuous at the spherical surface. Again applying these boundary conditions, but now to the general frequency-dependent electric field and dielectric displacement (Eq. 12), yields³⁹

$$\vec{E}_{RF}(\omega) = \frac{\Delta\vec{\mu}}{a^3} \frac{\epsilon_c + 2}{3} \frac{\epsilon(\omega) - 1}{\epsilon(\omega) + \frac{\epsilon_c}{2}}. \quad (13)$$

Here, ϵ_c as a constant value describes the fixed geometry of the solute, whereas $\epsilon(\omega)$ stands for the relaxation of the solvent. As an ionic liquid is composed of charged, dipolar molecules, its dielectric properties have to be described by the generalized permittivity³

$$\Sigma(\omega) = \epsilon(\omega) - 1 + \frac{4\pi i\sigma(\omega)}{\omega}, \quad (14)$$

where the dielectric conductivity $4\pi i\sigma(\omega)/\omega$ describes the creation of collective dipole moments by the mutual translational motion of charged species. This generalizes the constitutive relation to

$$\vec{P}(\vec{r}, \omega) = \frac{\Sigma(\omega)}{4\pi} \vec{E}(\vec{r}, \omega) \quad (15)$$

and the dielectric displacement to

$$\vec{D}(\vec{r}, \omega) = \vec{E}(\vec{r}, \omega) + 4\pi \vec{P}(\vec{r}, \omega) = (\Sigma(\omega) + 1) \vec{E}(\vec{r}, \omega). \quad (16)$$

In other words, for charged dipolar systems $\Sigma(\omega) + 1$ replaces $\epsilon(\omega)$ in Eq. 12 in case of neutral dipolar systems. Applying the same boundary conditions as above the reaction field can be generalized to

$$\vec{E}_{RF}(\omega) = \frac{\Delta\vec{\mu} \epsilon_c + 2}{a^3} \frac{\Sigma(\omega)}{\Sigma(\omega) + 1 + \frac{\epsilon_c}{2}}. \quad (17)$$

Generalizing the theory developed by Hsu *et al.*³⁹ for neutral dipolar solvents to the case of ionic liquids by replacing Eq. 13 with Eq. 17 we get the analogous expression for the solvation energy

$$\Delta U_{\Sigma}(t) = \frac{2}{\pi} \int_0^{\infty} \frac{\cos(\omega t)}{\omega} \text{Im} \left[\frac{\Sigma(\omega)}{\Sigma(\omega) + 1 + \frac{\epsilon_c}{2}} \right] d\omega. \quad (18)$$

Strictly speaking, the above equation should contain the dipolar energy $-(\Delta\vec{\mu}^2/a^3)((\epsilon_c + 2)/3)$ as a prefactor. However, when substituting $\Delta U(t)$ into Eq. 1, giving the solvation response function, the dipolar energy cancels out. Therefore, it is omitted in the above and following equations, where only the dimensionless part is retained.

B. Analytical calculation of the mean relaxation time of $S_{\Sigma}(t)$

At the global level, the most important property of the solvation response function $S_{\Sigma}(t)$ is its mean relaxation time

$$\tau_{\Sigma} = \int_0^{\infty} S_{\Sigma}(t) dt. \quad (19)$$

According to Eq. 1, $S_{\Sigma}(t)$ is calculated from the solvation energy ΔU_{Σ} at times t , zero and infinity. As the asymptotic value of $\Delta U_{\Sigma}(t)$ approaches values close to

zero (data not shown), its asymptotic value is omitted in order to simplify $S_{\Sigma}(t)$ to

$$S_{\Sigma}(t) \simeq \frac{\Delta U_{\Sigma}(t)}{\Delta U_{\Sigma}(0)}. \quad (20)$$

Consequently, the mean relaxation time is given by

$$\tau_{\Sigma} = \frac{T}{\Delta U_{\Sigma}(0)}, \quad (21)$$

where

$$T = \int_0^{\infty} \Delta U_{\Sigma}(t) dt = \quad (22)$$

$$= \lim_{\omega \rightarrow 0} \frac{1}{\omega} \text{Im} \left[\frac{\Sigma(\omega)}{\Sigma(\omega) + 1 + \frac{\epsilon_c}{2}} \right] = \quad (23)$$

$$= \lim_{\omega \rightarrow 0} \frac{1}{\omega} \frac{(1 + \frac{\epsilon_c}{2}) \Sigma''(\omega)}{(\Sigma'(\omega) + 1 + \frac{\epsilon_c}{2})^2 + (\Sigma''(\omega))^2}. \quad (24)$$

With

$$\Sigma(\omega) = \epsilon(\omega) - 1 + \frac{4\pi i\sigma(\omega)}{\omega} \quad (25)$$

$$\Sigma(\omega) = \Sigma'(\omega) + i\Sigma''(\omega) \quad (26)$$

$$\epsilon(\omega) = \epsilon'(\omega) + i\epsilon''(\omega) \quad (27)$$

$$\sigma(\omega) = \sigma'(\omega) + i\sigma''(\omega). \quad (28)$$

Eq. 24 can be rewritten upon substitution as

$$T = \lim_{\omega \rightarrow 0} \frac{1}{\omega} \text{Im} \left[\frac{\Sigma(\omega)}{\Sigma(\omega) + 1 + \frac{\epsilon_c}{2}} \right] = \quad (29)$$

$$= \lim_{\omega \rightarrow 0} \frac{(1 + \frac{\epsilon_c}{2})(\epsilon''(\omega)\omega + 4\pi\sigma'(\omega))}{(\omega(\epsilon'(\omega) + \frac{\epsilon_c}{2}) - 4\pi\sigma''(\omega))^2 + (\omega\epsilon''(\omega) + 4\pi\sigma'(\omega))^2} \quad (30)$$

$$= \lim_{\omega \rightarrow 0} \frac{(1 + \frac{\epsilon_c}{2})4\pi\sigma'(\omega)}{(-4\pi\sigma''(\omega))^2 + (4\pi\sigma'(\omega))^2} \quad (31)$$

$$= \lim_{\omega \rightarrow 0} (1 + \frac{\epsilon_c}{2}) \frac{1}{4\pi\sigma'(\omega)} \quad (32)$$

$$= (1 + \frac{\epsilon_c}{2}) \frac{1}{4\pi\sigma_0}. \quad (33)$$

When proceeding from Eq. 30 to 31 we have omitted all terms involving $\epsilon'(\omega)$ and $\epsilon''(\omega)$ as they are multiplied by ω and thus vanish in the zero-frequency limit. Furthermore, $\lim_{\omega \rightarrow 0} \sigma''(\omega) = 0$.

As can be seen from Eq. 21, the calculation of the mean relaxation time needs both, the time integral (see. Eq. 22) and the amplitude $\Delta U_{\Sigma}(0)$. For $t = 0$ Eq. 18 becomes

$$\Delta U_{\Sigma}(0) = \frac{2}{\pi} \int_0^{\infty} \frac{1}{\omega} \text{Im} \left[\frac{\Sigma(\omega)}{\Sigma(\omega) + 1 + \frac{\epsilon_c}{2}} \right] d\omega. \quad (34)$$

Following the elegant formalism described by Rips *et al.*⁴⁰, we get

$$\Delta U_{\Sigma}(0) = \lim_{\omega \rightarrow 0} \left[\frac{\Sigma(\omega)}{\Sigma(\omega) + 1 + \frac{\epsilon_c}{2}} \right] - \lim_{\omega \rightarrow \infty} \left[\frac{\Sigma(\omega)}{\Sigma(\omega) + 1 + \frac{\epsilon_c}{2}} \right] \quad (35)$$

Using Eqs. 25-28, the infinite-frequency limit above gives

$$\lim_{\omega \rightarrow \infty} \left[\frac{\Sigma(\omega)}{\Sigma(\omega) + 1 + \frac{\epsilon_c}{2}} \right] = \frac{2(\epsilon_\infty - 1)}{2(\epsilon_\infty - 1) + \epsilon_c + 2}, \quad (36)$$

while the zero-frequency limit gives unity. Altogether, the amplitude becomes

$$\Delta U_\Sigma(0) = \frac{\epsilon_c + 2}{\epsilon_c + 2\epsilon_\infty}. \quad (37)$$

Combining Eqs. 33 and 37 we get the mean relaxation time

$$\tau_\Sigma = \frac{T}{\Delta U_\Sigma(0)} = \frac{\epsilon_c + 2\epsilon_\infty}{2} \frac{1}{4\pi\sigma_0}. \quad (38)$$

This shows that τ_Σ is determined only by three parameters, namely ϵ_c , σ_0 and ϵ_∞ . ϵ_c characterizes the polarizability of the solute, σ_0 stands for the translational mobility of the solvent environment and ϵ_∞ describes the polarizability of the solvent. Although the above derivation differs in parts, we get the same analytical result for the mean relaxation time as Zhang *et al.*⁶

C. Using components of the dielectric spectrum to calculate the solvation response function

While experiments always yield the dielectric spectrum as an inseparable entity, except for the static conductivity σ_0 , which is also accessible from other experimental methods, simulation studies offer the possibility to analyze how different components of the computational spectrum determine the shape of the solvation response function $S(t)$. For conducting systems, the hyperbola $4\pi i\sigma_0/\omega$ dominates the imaginary part of the generalized dielectric permittivity $\Sigma(\omega)$. Therefore, it is usually subtracted:

$$\begin{aligned} \Sigma_0(\omega) &= \Sigma(\omega) - \frac{4\pi i\sigma_0}{\omega} \\ &= \epsilon(\omega) - 1 + \frac{4\pi i(\sigma(\omega) - \sigma_0)}{\omega}. \end{aligned} \quad (39)$$

The complement $\Sigma_0(\omega)$ of the conductivity hyperbola $4\pi i\sigma_0/\omega$ is representative of the fine structure of the spectrum. Its role can be highlighted by reducing Eq. 18 to

$$\Delta U_{\Sigma_0}(t) = \frac{2}{\pi} \int_0^\infty \frac{\cos(\omega t)}{\omega} \text{Im} \left[\frac{\Sigma_0(\omega)}{\Sigma_0(\omega) + 1 + \frac{\epsilon_c}{2}} \right] d\omega. \quad (40)$$

The subtraction of $4\pi i\sigma_0/\omega$ corresponds to the replacement of $\sigma'(\omega)$ with $(\sigma'(\omega) - \sigma_0)$ in Eq. 32:

$$\int_0^\infty \Delta U_{\Sigma_0}(t) dt = \lim_{\omega \rightarrow 0} \left(1 + \frac{\epsilon_c}{2} \right) \frac{1}{4\pi(\sigma'(\omega) - \sigma_0)}. \quad (41)$$

Unfortunately, this integral diverges. In other words, the inclusion of the conductivity hyperbola is essential for

this model theory.⁷ Because of its fundamental role, it makes sense to study the influence of $4\pi i\sigma_0/\omega$ separately, simplifying Eq. 18 to

$$\Delta U_{\sigma_0}(t) = \frac{2}{\pi} \int_0^\infty \frac{\cos(\omega t)}{\omega} \text{Im} \left[\frac{\frac{4\pi i\sigma_0}{\omega}}{\frac{4\pi i\sigma_0}{\omega} + 1 + \frac{\epsilon_c}{2}} \right] d\omega \quad (42)$$

$$= \frac{2}{\pi} \int_0^\infty \cos(\omega t) \frac{T}{1 + (\omega T)^2} d\omega \quad (43)$$

$$= e^{-t/T} \quad (44)$$

with the relaxation time

$$T = \left(1 + \frac{\epsilon_c}{2} \right) \frac{1}{4\pi\sigma_0}. \quad (45)$$

In other words, the conductivity hyperbola - when taken solely - leads to a mono-exponential function. To get a more realistic $S(t)$, the logical next step is to replace the static conductivity σ_0 by its frequency-dependent analogue $\sigma(\omega)$, yielding

$$\Delta U_\sigma(t) = \frac{2}{\pi} \int_0^\infty \frac{\cos(\omega t)}{\omega} \text{Im} \left[\frac{\frac{4\pi i\sigma(\omega)}{\omega}}{\frac{4\pi i\sigma(\omega)}{\omega} + 1 + \frac{\epsilon_c}{2}} \right] d\omega, \quad (46)$$

representing the complete translational contribution. Referring to Eq. 31 it is clear that this replacement does not affect T . Thus we have shown that T is universal for all three cases discussed. The amplitudes, however, differ. Repeating the calculation in Eq. 35 for $4\pi i\sigma_0/\omega$ or $4\pi i\sigma(\omega)/\omega$ instead of $\Sigma(\omega)$ we get $\Delta U_{\sigma_0}(0) = \Delta U_\sigma(0) = 1$. Hence, the mean relaxation time for these two cases is $\tau_{\sigma_0} = \tau_\sigma = T$ as opposed to Eq. 38. We anticipate from the results shown later, that time dependence of $S_{\sigma_0}(t)$ and $S_\sigma(t)$ is rather different, although the respective mean relaxation times are identical.

D. Describing the solute using an ellipsoidal cavity

All previous expressions are based on a spherical cavity containing the solute. As the studied solute Coumarin 153 is rather anisotropic in shape it seems prudent to make the cavity anisotropic as well. Following previous works using reaction field methods with an ellipsoidal solute cavity in polar liquids,^{39,41-43} we applied this approach to ionic liquids. The response function in this case is given by

$$F(\omega) = \begin{pmatrix} f_a(\omega) & 0 & 0 \\ 0 & f_b(\omega) & 0 \\ 0 & 0 & f_c(\omega) \end{pmatrix}, \quad (47)$$

where

$$f_i = \frac{3A_i(1 - A_i)\Sigma(\omega)}{1 + \Sigma(\omega)(1 - A_i)}, \quad i = a, b, c \quad (48)$$

describe the response function along the three axes of the ellipsoid and A_i are ellipsoidal shape factor integrals.⁴¹

The solvation energy is then given by

$$\Delta U(t) = -\frac{\epsilon_c + 2}{3abc} \Delta\mu \cdot \frac{2}{\pi} \int_0^\infty \frac{\cos(\omega t)}{\omega} \text{Im}[F(\omega)] d\omega \cdot \Delta\mu. \quad (49)$$

III. METHODS

The results presented here were gathered from polarizable molecular dynamics simulations of three different ionic liquids, 1-ethyl-3-methylimidazolium tetrafluoroborate (EMIM⁺BF₄⁻), 1-ethyl-3-methylimidazolium trifluoromethanesulfonate (EMIM⁺TfO⁻) and 1-butyl-3-methylimidazolium tetrafluoroborate (BMIM⁺BF₄⁻), each containing 1000 ion pairs and a single coumarin 153 (C153) molecule with a charge distribution reflecting its electronic ground state. All simulations were run at a temperature of 300K in cubic boxes with respective box lengths of 64.4Å for EMIM⁺BF₄⁻, 67.9Å for EMIM⁺TfO⁻ and 68.65Å for BMIM⁺BF₄⁻ using a time step of 0.5 fs. Non-bonded interactions were calculated using the Lennard-Jones potential with a switch function between 11 and 12Å and the PME method^{44,45} with a real-space cut-off of 12Å and a κ of 0.41 Å⁻¹. The lengths of all bonds involving a hydrogen atom were held fixed by the SHAKE algorithm.⁴⁶ The charge distribution of the solvent molecules was made polarizable by adding Drude particles to all non-hydrogen atoms.⁴⁷ These simulations are the same as in Ref. 10, where more detailed information on the computational setup is given. For each system, 60 ns of trajectory data containing only coordinates and additional 15 ns of trajectory data also containing velocities were produced using the molecular dynamics package CHARMM⁴⁸. For a quantification of the various solvation response functions we fitted them to the function

$$S(t) \approx ae^{-t/\tau_1} + (1-a)e^{-(t/\tau_2)^\beta}, \quad (50)$$

consisting of an exponential and a Kohlrausch-William-Watts (KWW) function.^{10,12,25,35} The set of parameters is collected in Table I.

IV. RESULTS AND DISCUSSION

A. Dielectric spectra

The dielectric relaxation data shown in Fig. 1 was calculated from molecular dynamics simulation data following the approach used in previous work.³ The time correlation functions of the total rotational dipole moment ($\langle \vec{M}_D(0) \cdot \vec{M}_D(t) \rangle$), the total current ($\langle \vec{J}(0) \cdot \vec{J}(t) \rangle$) and their cross-correlation function ($\langle \vec{M}_D(0) \cdot \vec{J}(t) \rangle$) were fitted using fit functions of the form

$$f(t) \approx \sum_j A_j \cdot e^{-t/\tau_j} + \sum_k A_k \cos(\omega_k t + \delta_k) \cdot e^{-t/\tau_k}, \quad (51)$$

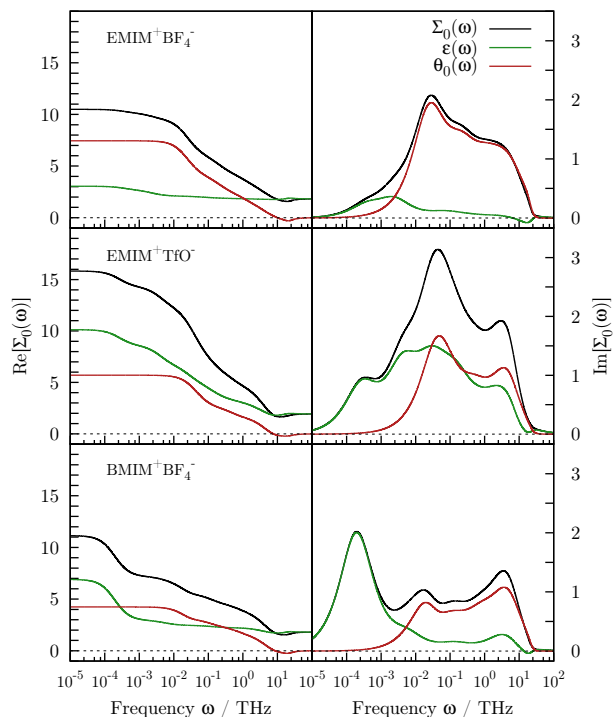


FIG. 1. Dielectric relaxation functions (cf. Eq. 39) generated from MD simulation data, real (left column) and imaginary parts (right column).

where $f(t)$ denotes the respective time correlation function. In order to achieve a more reliable value for the longest time constant of $\langle \vec{J}(0) \cdot \vec{J}(t) \rangle$,³ the relationship

$$\frac{d^2}{dt^2} \langle (\Delta \vec{M}_J(t))^2 \rangle = 2 \langle \vec{J}(0) \cdot \vec{J}(t) \rangle \quad (52)$$

described in Ref. 49 was practically applied. As $\langle (\Delta \vec{M}_J(t))^2 \rangle$ could be calculated from the much longer coordinate trajectory, $\langle \vec{J}(0) \cdot \vec{J}(t) \rangle$ gained by calculating the second derivative using the Savitzky-Golay algorithm⁵⁰ proved to be consistent with the directly calculated correlation function (cf. Fig. S1 provided in the Supplementary Material). This provided another source for the above-mentioned longest time constant. Tables S1, S2 and S3 in the Supplementary Material list all the fit parameters used here.

B. Characterization of the solvation response function within the reaction field continuum model

1. The time dependence

As we have already learned in Eq. 41, the static conductivity σ_0 is of central importance when applying the reaction field continuum model (RFCM) to conducting systems. Therefore, we study its properties first. The

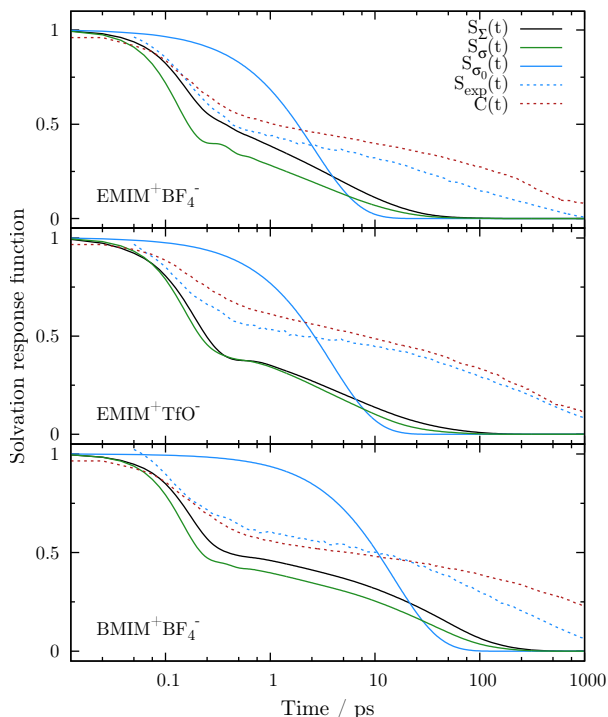


FIG. 2. Comparison of $S_{\Sigma}(t)$ (black, cf. Eq. 18), $S_{\sigma}(t)$ (green, cf. Eq. 46), $S_{\sigma_0}(t)$ (blue, cf. Eq. 44), $C(t)$ (dotted red, cf. Eq. 57) and experimental data⁷ (dotted light blue). While $S_{\sigma_0}(t)$ is a simple mono-exponential curve, $S_{\sigma}(t)$ already shows the typical differentiation into two distinct time domains. The addition of rotational motion in $S_{\Sigma}(t)$, i.e. taking whole $\Sigma(\omega)$, changes the curve only slightly. Comparison to $S_{exp}(t)$ (cf. Ref. 7) and $C(t)$ shows, that the solvation response function predicted by the RFCM decays too fast.

values calculated for the three systems studied here are 0.402 S/m, 0.279 S/m and 0.069 S/m for $\text{EMIM}^+\text{BF}_4^-$, $\text{EMIM}^+\text{TfO}^-$ and $\text{BMIM}^+\text{BF}_4^-$, respectively. $S_{\sigma_0}(t)$ is a mono-exponential function (see Eq. 44 and Fig. 2). This, however, does not reflect the typical two time regimes of the solvation response function in ionic liquids.

The next logical step is the full frequency-dependent conductivity $\sigma(\omega)$. In fact, this extension already generates two time regimes in the solvation response function, as can be seen in Fig. 2 and Table I. When compared to the mono-exponential function typical for the static conductivity, $S_{\sigma}(t)$ already has a shape that can be modeled by the fit function Eq. 50. As the actual amplitudes derived from the fit are almost equal, we are facing a one-to-one mixture of an exponential and a KWW function.

With the above description, the essentials of translational motion are represented within the RFCM. In order to include rotational motion, we replace $4\pi i\sigma(\omega)/\omega$ by $\Sigma(\omega)$ and use Eq. 18. This changes $S(t)$ quantitatively, but not qualitatively, as can be seen in Fig. 2 and Table I. The inclusion of $\epsilon(\omega) - 1$, i.e. the change from $S_{\sigma}(t)$

to $S_{\Sigma}(t)$, changes the fit parameters (cf. Eq. 50) only to a minor degree, except for the change in β in the case of $\text{EMIM}^+\text{TfO}^-$. This shows in a compact way the importance of $\epsilon(\omega)$ for $\text{EMIM}^+\text{TfO}^-$, which is evident from its spectrum in Fig. 1.

2. The mean relaxation time

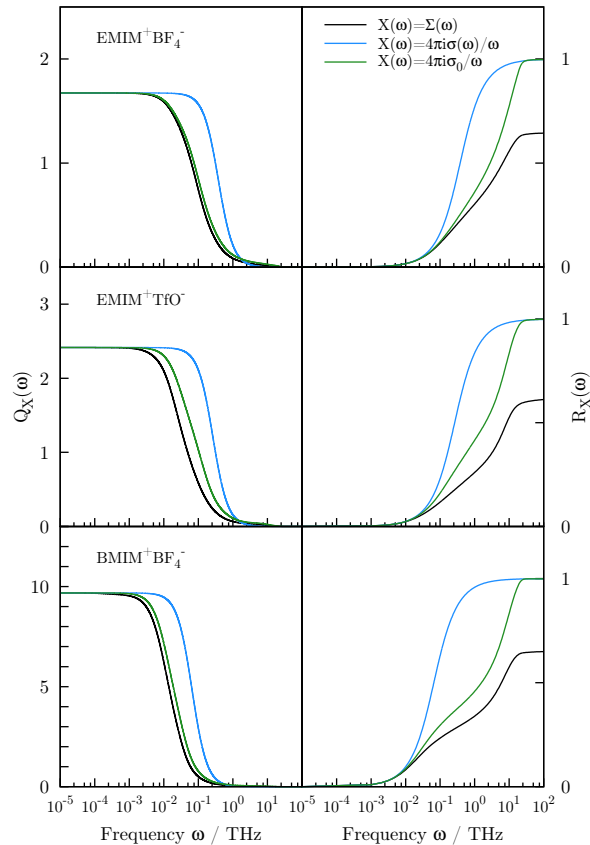


FIG. 3. The left column shows the integrands $Q_X(\omega)$ with $X(\omega) = \{\Sigma(\omega), 4\pi i\sigma(\omega)/\omega, 4\pi i\sigma_0/\omega\}$ (cf. Eq. 53). The zero-frequency limit corresponds to the time integral T (see Eq. 22). The right column shows the running integral $R_X(\omega)$ of the corresponding curves in the left column (see Eq. 54). The last values of these integrals correspond to $\Delta U_X(0)$ and are the amplitudes in Eq. 21.

The qualitative description of the time dependence of $S(t)$ given above is now accompanied by a quantification in terms of the mean relaxation time τ (cf. Eqs. 21, 22 and 34). Thus, for the calculation of τ one needs the time integral of $\Delta U(t)$, which corresponds to the zero-frequency limit in Eq. 23, as well as the amplitude $\Delta U(0)$, given by the integral in the frequency domain

(see Eq. 34). The respective integrand

$$Q_X(\omega) = \frac{1}{\omega} \frac{X(\omega)}{X(\omega) + 1 + \frac{\epsilon_c}{2}} \quad (53)$$

and its running integral

$$R_X(\omega) = \int_0^\omega Q_X(\omega') d\omega' \quad (54)$$

are shown in Fig. 3 for the three cases $X(\omega) = \{\Sigma(\omega), 4\pi i\sigma(\omega)/\omega, 4\pi i\sigma_0/\omega\}$. The integrands in the left column of Fig. 3 are different, but their zero-frequency limit, i.e. the time integral T , is the same. This confirms numerically the analytical results found in Secs. II B and II C. The running integrals $R_X(\omega)$ are shown on the right side of Fig. 3. Their asymptotic limits give the amplitudes $\Delta U_X(0)$. In accordance with Sec. II C, $\Delta U_{\sigma_0}(0)$ and $\Delta U_\sigma(0)$ both are unity and $\Delta U_\Sigma(0)$ can be calculated from Eq. 37, which can be rewritten as

$$\frac{1}{\Delta U_\Sigma(0)} = \frac{\epsilon_c + 2\epsilon_\infty}{\epsilon_c + 2} = \quad (55)$$

$$= 1 + \frac{2(\epsilon_\infty - 1)}{\epsilon_c + 2}. \quad (56)$$

In a system consisting of non-polarizable molecules, i.e. $\epsilon_\infty = 1$, the amplitude also becomes $1/\Delta U_\Sigma(0) = 1$. Consequently, at all three levels of complexity the mean relaxation time becomes the very same. In the present case, though, the simulations were performed with a polarizable force field characterized by the following optical dielectric constants ϵ_∞ : 1.749 (EMIM⁺BF₄⁻), 1.906 (EMIM⁺TfO⁻) and 1.742 (BMIM⁺BF₄⁻). This leads to amplitudes lower than 1 (see Fig. 3) and thus enhances the mean relaxation times by about 40-50%. Inspecting Eq. 56 shows that only the asymptotic value of $\epsilon(\omega)$ enters the amplitude. Thus, the complete spectrum $\epsilon(\omega)$ is diminished by the dielectric conductivity $4\pi i\sigma(\omega)/\omega$, when considering the mean relaxation time.

The mean relaxation times of $S_{\sigma_0}(t)$ and $S_\sigma(t)$ are identical, as both, the time integral T as well as the amplitudes are equal (see Fig. 3). In other words, the static conductivity describes $S_\sigma(t)$ exactly on the average, but not in detail.

3. Comparison to simulated and experimental solvation response functions

So far, our considerations of the solvation response function were limited to the framework of the reaction field continuum theory. Now, we contrast these results with experiment⁷ and simulation. In the latter case, we do not refer to the non-equilibrium simulation, but we have calculated¹⁰ the solvation response function from equilibrium molecular dynamics (MD) simulation data as the time correlation function

$$C(t) = \frac{\langle \delta\Delta U(0)\delta\Delta U(t) \rangle}{\langle \delta\Delta U(0)^2 \rangle}, \quad (57)$$

where $\delta\Delta U(t)$ describes the fluctuations of the solvation energy difference between the two electronic states of the solute. The results are shown in Fig. 2 in comparison to the triple of continuum-based functions and experimental data.⁷ The pair of the directly calculated functions $C(t)$ (see Eq. 57) and those computed indirectly via inserting simulated dielectric spectra into the reaction field continuum model behaves much like their experimental analogues (cf. Fig. 9 of Ref. 7): The simple continuum model gives a solvation response function with the characteristic separation into two time regimes. The fast-decaying sub-picosecond regime of the solvation response is modeled rather well for EMIM⁺BF₄⁻ and BMIM⁺BF₄⁻, but not for EMIM⁺TfO⁻, while the long-time regime is decaying much too fast in all three liquids. The striking similarity of curves derived from either the experimental or computational spectra demonstrates that deviations are almost independent of the source of the dielectric spectrum, but rather show up the limitations of the reaction field continuum model. Table I lists the fit parameters used to describe the various solvation response functions calculated from the continuum model in comparison to the linear response time correlation function used in Ref. 10 and experimental data.⁷

4. Retarding relaxation within the framework of RFCM

Both in simulation and experiment^{7,32}, RFCM correctly models the dualistic shape of the solvation response function in a qualitative way. However, at the quantitative level clear deficiencies of the model theory are visible. In particular, in the long-time regime the solvation response function decays too fast. Eqs. 33 and 45 offer a possibility for retardation. The time integral T_X represents the area under the curve $\Delta U_X(t)$ and is thus proportional to the mean relaxation time. For a monotonic time function, any enhancement of its integral automatically elevates the whole curve. Therefore, the parameters ϵ_c and σ_0 entering T_X are a direct route to manipulate $S(t)$ both in its shape and its integral properties. At the experimental side an effective conductivity $\sigma_0^{eff} = \frac{\sigma_0}{2.4}$ was determined for a series of ionic liquids.^{6,32} In order to be consistent with these findings, we use the same scaling factor here. The results are shown in Fig. 4 (green curves). A further deficiency of the RFCM is the fact that structural and electrostatic properties of the solute do not enter at all, if $\epsilon_c = 1$, meaning that the solute is not polarizable. An increase in ϵ_c corresponds to enhancing the polarizability of the solute. Assembling the molecular polarizability of C153 from its atomic polarizabilities according to Ref. 51 and converting it to ϵ_c via the Clausius-Mosotti equation we get a tentative value of $\epsilon_c = 3$. Therefore, Fig. 4 shows curves for the triple $\epsilon_c = 1, 2, 3$. The value $\epsilon_c = 2$ was included, because it was used in experimental studies.^{6-9,32}

As can be seen in Fig. 4, both, a higher ϵ_c as well as using σ_0^{eff} instead of σ_0 leads to an elevation of $S(t)$.

TABLE I. A list of all fit parameters used to describe the different variants of $S_X(t)$, $S_{exp}(t)$ and $C(t)$. The value of ϵ_c describes the polarizability of C153 within the RFCM (see Eq. 9). $\sigma_0^{eff} = \sigma_0/2.4$ denotes an effective, empirically determined^{6,9,32} static conductivity. Graphical representations of the functions listed here can be found in Figs. 2, 4 and 6.

		ϵ_c	σ_0/σ_0^{eff}	a	τ_1 / ps	τ_2 / ps	β	τ_X / ps
EMIM⁺BF₄⁻	$S_{\sigma_0}(t)$	1	σ_0	1.0	2.63	-	-	2.63
	$S_{\sigma}(t)$	1	σ_0	0.55	0.138	3.41	0.58	2.63
	$S_{\Sigma}(t)$	1	σ_0	0.42	0.189	4.27	0.58	4.08
	$S_{\Sigma}(t)$	2	σ_0	0.37	0.209	4.95	0.60	4.95
	$S_{\Sigma}(t)$	3	σ_0	0.33	0.225	5.69	0.61	5.83
	$S_{\Sigma}(t)$	1	σ_0^{eff}	0.45	0.206	9.88	0.54	9.75
	$S_{\Sigma}(t)$	2	σ_0^{eff}	0.40	0.232	11.8	0.55	11.8
	$S_{\Sigma}(t)$	3	σ_0^{eff}	0.37	0.256	13.8	0.57	13.9
	$C(t)^{10}$	-	-	0.45	0.238	217	0.40	397
	$S_{exp}(t)^7$	-	-	0.55	0.269	87.2	0.52	73.3
	$S_{ell}(t)$	1	σ_0	0.46	0.177	3.94	0.58	3.58
	$S_{ell}^a(t)$	1	σ_0	0.46	0.176	3.93	0.58	3.58
	$S_{ell}^b(t)$	1	σ_0	0.43	0.186	4.19	0.58	3.95
	$S_{ell}^c(t)$	1	σ_0	0.36	0.212	5.08	0.60	5.11
EMIM⁺TfO⁻	$S_{\sigma_0}(t)$	1	σ_0	1.0	3.79	-	-	3.79
	$S_{\sigma}(t)$	1	σ_0	0.50	0.147	4.53	0.58	3.79
	$S_{\Sigma}(t)$	1	σ_0	0.48	0.169	5.81	0.50	6.18
	$S_{\Sigma}(t)$	2	σ_0	0.43	0.187	6.59	0.51	7.44
	$S_{\Sigma}(t)$	3	σ_0	0.39	0.201	7.48	0.52	8.70
	$S_{\Sigma}(t)$	1	σ_0^{eff}	0.55	0.193	15.7	0.48	14.7
	$S_{\Sigma}(t)$	2	σ_0^{eff}	0.51	0.223	18.7	0.50	17.7
	$S_{\Sigma}(t)$	3	σ_0^{eff}	0.48	0.252	21.8	0.51	20.7
	$C(t)^{10}$	-	-	0.32	0.285	227	0.37	646
	$S_{exp}(t)^7$	-	-	0.45	0.233	277	0.49	317
	$S_{ell}(t)$	1	σ_0	0.52	0.158	5.44	0.49	5.48
	$S_{ell}^a(t)$	1	σ_0	0.52	0.158	5.43	0.49	5.46
	$S_{ell}^b(t)$	1	σ_0	0.49	0.167	5.71	0.50	6.00
	$S_{ell}^c(t)$	1	σ_0	0.42	0.189	6.74	0.51	7.67
BMIM⁺BF₄⁻	$S_{\sigma_0}(t)$	1	σ_0	1.0	15.2	-	-	15.2
	$S_{\sigma}(t)$	1	σ_0	0.58	0.161	27.6	0.68	15.2
	$S_{\Sigma}(t)$	1	σ_0	0.53	0.196	38.5	0.70	23.2
	$S_{\Sigma}(t)$	2	σ_0	0.48	0.222	43.7	0.72	28.2
	$S_{\Sigma}(t)$	3	σ_0	0.44	0.245	48.9	0.73	33.2
	$S_{\Sigma}(t)$	1	σ_0^{eff}	0.56	0.233	99.7	0.71	52.6
	$S_{\Sigma}(t)$	2	σ_0^{eff}	0.52	0.275	113	0.73	63.5
	$S_{\Sigma}(t)$	3	σ_0^{eff}	0.49	0.319	127	0.76	74.0
	$C(t)^{10}$	-	-	0.40	0.245	1260	0.31	6070
	$S_{exp}(t)^7$	-	-	0.38	0.266	202	0.52	233.7
	$S_{ell}(t)$	1	σ_0	0.56	0.181	35.7	0.69	20.4
	$S_{ell}^a(t)$	1	σ_0	0.56	0.181	35.6	0.69	20.3
	$S_{ell}^b(t)$	1	σ_0	0.53	0.192	37.8	0.70	22.5
	$S_{ell}^c(t)$	1	σ_0	0.47	0.226	44.7	0.72	29.1

However, the influence of ϵ_c is focused on short and medium times, while σ_0^{eff} mainly affects the long-time domain. Thus, simultaneously increasing ϵ_c and using σ_0^{eff} allows to manipulate $S(t)$ on the whole time scale. The best example is BMIM⁺BF₄⁻, where σ_0^{eff} combined with $\epsilon_c = 3$ gives reasonable agreement with experimental curves. A similarly good agreement is found in the case of EMIM⁺BF₄⁻, while for EMIM⁺TfO⁻ the improvement is largely confined to the initial region of $S(t)$.

Table I lists the fit parameters and mean relaxation

times τ_X (last column) for $S_{\Sigma}(t)$ as a function of ϵ_c and σ_0 . A stringent feature across the three liquids studied here is that the variation in ϵ_c and/or σ_0 primarily affects τ_2 , while β and the amplitude a stays almost constant and τ_1 shows only modest change. Although numerically evaluated the mean relaxation times τ_X exactly follow Eq. 38. Approximately, τ_2 also follows this relation. However, this comes from the special values of parameters β and a . For the KWW part of the fit function the contribution to the mean relaxation time is given by $\langle\tau\rangle = ((1-a)/\beta)\Gamma(1/\beta)\tau_2$. If β and a are close to 0.5, as

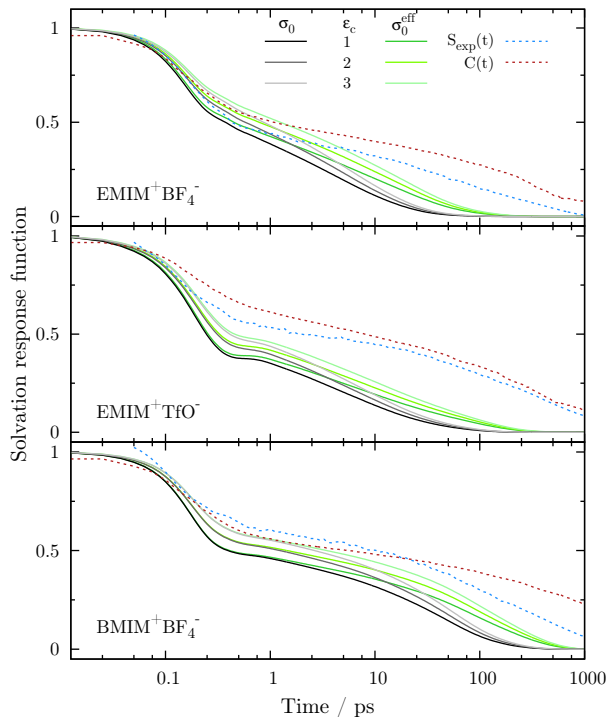


FIG. 4. Variation of ϵ_c from 1 to 3 in combination with σ_0 (black curves) or $\sigma_0^{eff} = \sigma_0/2.4$ (green curves, for the factor 2.4 cf. Refs. 6, 32 and 9) in comparison to results from simulation¹⁰ (red dotted line) and experiment⁷ (blue dotted line). Increasing ϵ_c lifts the curves mainly for short and medium times, while using σ_0^{eff} instead of σ_0 slows down the decay in the long-time domain.

is the case for $\text{EMIM}^+\text{BF}_4^-$ and $\text{EMIM}^+\text{TfO}^-$, $\tau_X \approx \tau_2$.

5. Linking the time behaviour of $S(t)$ with the imaginary part of the dielectric spectrum

Although usually subtracted, the conductivity hyperbola $4\pi i\sigma_0/\omega$ is an essential feature of the imaginary part of the dielectric spectrum of conducting systems. Within the framework of RFCM, we have learned above in Eq. 41 that the conductivity hyperbola has to be included to avoid divergence of the time integral. As can be seen in Fig. 5 this has dramatic consequences for $\text{Im}[\Sigma(\omega)] = \Sigma''(\omega)$: In the low-frequency region of the spectrum the intrinsic part $\Sigma_0(\omega)$ is completely swamped by the hyperbola, as its values exceed those of $\Sigma_0(\omega)$ by many orders of magnitude. The effect that the peaks at low frequencies do not significantly contribute to the RFCM can also be observed in Fig. 3, where the integrands in the left column begin to differ only beyond a certain frequency threshold and the zero-frequency limit is determined only by the static conductivity (cf. Eqs. 29-33 and 45). In contrast, this is not the case in the high-frequency region of the spectrum, which is the same

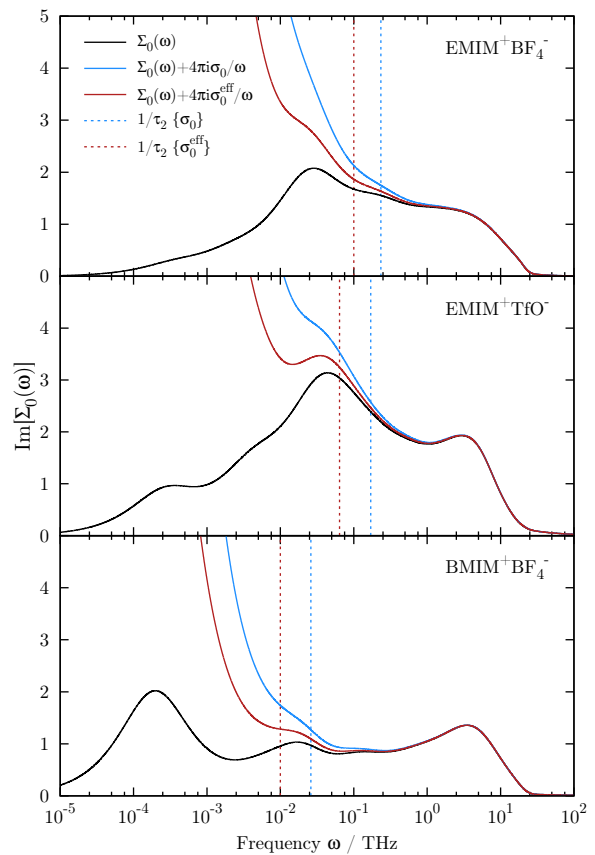


FIG. 5. The imaginary part of $\Sigma_0(\omega)$ by itself (black curve) and after addition of the conductivity hyperbola using either the unscaled σ_0 (blue curve) or the scaled $\sigma_0^{eff} = \sigma_0/2.4$ (red curve). The two curves including the static conductivity diverge quickly as ω becomes smaller. The fine structure of the peaks at low frequencies ($\omega < 10^{-2}$ THz) is quickly diminished by the hyperbola, especially as this graph is plotted on a semilog scale. The vertical dotted lines mark $\omega_2 = 1/\tau_2$, when either using the unscaled conductivity σ_0 (dashed blue line) or the scaled σ_0^{eff} (dashed red line).

for $\Sigma_0(\omega)$ and $\Sigma(\omega)$. Here, the characteristic feature of the spectra of all three systems is a peak at ≈ 4 THz. In the time domain this corresponds to a relaxation time of ≈ 0.25 ps. This value is close to the τ_1 values in Table I, which shows only modest variation across systems and model parameters.

As illustrated by Fig. 5 a threefold partitioning of the frequency range is possible: $\Sigma(\omega) \gg \Sigma_0(\omega)$, $\Sigma(\omega) \approx \Sigma_0(\omega)$ and $\Sigma(\omega) = \Sigma_0(\omega)$, classified low, medium and high in the following. In this medium region, the fine structure of $\Sigma_0(\omega)$ emerges to an extent depending on the value of the static conductivity. Using σ_0^{eff} instead of σ_0 shifts the medium region towards lower frequencies. Consequently, characteristic features of $\Sigma_0(\omega)$ become noticeable in $\Sigma(\omega)$. This goes along with the retardation of $S(t)$ (cf. Fig. 4), which can be focused on τ_2 ,

as we have learned above (cf. Table I). We emphasize that τ_2 and (the almost constant) β from the KWW part of the fit function describe a stretched exponential representing the superposition of many exponentials. The corresponding frequency $\omega_2 = 1/\tau_2$ is given as a vertical dotted bar in Fig. 5 for σ_0 and σ_0^{eff} with $\epsilon_c = 1$. In fact, ω_2 marks the beginning of the high-frequency region, where the differences between $\Sigma_0(\omega)$ and $\Sigma(\omega)$ have disappeared. When using σ_0^{eff} instead of σ_0 , ω_2 shifts downwards synchronously with the conductivity hyperbola.

Taking the arguments above together, one understands why the RFCM produces reasonably good agreement in the short-time regime, while decaying too fast for longer times. In particular in the case of $\text{EMIM}^+\text{TfO}^-$, $\Sigma(\omega)$ lacks spectral information of $\Sigma_0(\omega)$ across a wide frequency range, which cannot be repaired sufficiently by rescaling σ_0 . As the latter is considerably lower for $\text{BMIM}^+\text{BF}_4^-$ when compared to the other two systems, a wider range of the spectrum is covered by $\Sigma(\omega)$. Therefore, in this case RFCM agrees much better with simulation and experiment.

C. Anisotropy in charge distribution and shape

All above considerations refer to dipolar solute enclosed in a spherical cavity. Within the RFCM the dipole moment and the radius of the sphere are, except for ϵ_c , the only parameters describing the solute. As they both enter as prefactors, they cancel out upon normalization. In order to include more detailed features of the solute, we modified RFCM in two ways. First, the steric anisotropy of the solute was modeled by replacing the spherical cavity with an ellipsoid,^{39,43} resulting in Eq. 49. The principal axes of the solute were aligned with the coordinate system and a bounding box parallel to these axes was erected. This gave the relative lengths of the axes a , b and c of the ellipsoid. Subsequently, a , b and c were rescaled so that the volume of the ellipsoid equals the Voronoi volume of C153, yielding $a=7.00 \text{ \AA}$, $b=4.66 \text{ \AA}$ and $c=2.85 \text{ \AA}$. The corresponding ellipsoidal shape factor integrals⁴¹ are $A_a=0.18$, $A_b=0.30$, $A_c=0.52$. The change in dipole moment upon excitation $\Delta\vec{\mu}$ of the solute was projected onto the principal axes, giving the components $\Delta\mu_a=-1.24 e\text{\AA}$, $\Delta\mu_b=0.12 e\text{\AA}$, $\Delta\mu_c=-0.02 e\text{\AA}$. Since $\Delta\mu_a$ exceeds $\Delta\mu_b$ by an order of magnitude and $\Delta\mu_c$ by another one, the dipolar energy is essentially given by the prefactor $\frac{\Delta\mu_a^2}{abc}$. The only difference to the spherical cavity comes from $A_a \neq \frac{1}{3}$. As can be seen in Fig. 6 and Table I, the deviations from the spherical model are marginal. Table I rationalizes that the a -axis of the ellipsoid essentially determines the time dependence as a whole. This comes from the fact that the a -axis and $\Delta\vec{\mu}$ are almost collinear. Thus, the solute behaves as if it were spherical.

A second possibility to include anisotropic features of C153 is the inclusion of higher multipole moments of the

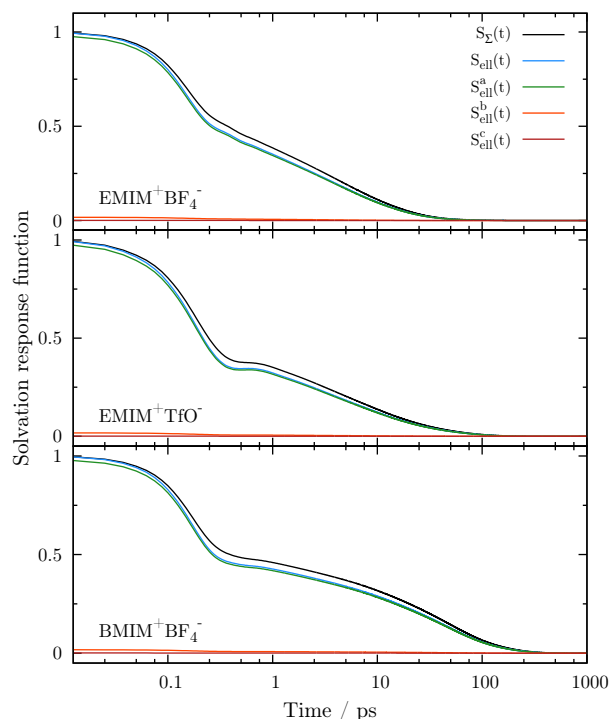


FIG. 6. Solvation response function using the model with an ellipsoidal cavity. The black curve shows the response using a spherical cavity. The total response with an ellipsoidal cavity in blue, the contribution of principal component a in green, the contribution of principal component b in orange and the contribution of principal component c in red.

solute in the RFCM, see Eq. 3. We have included the quadrupole moment, however changes were marginal as well (data not shown).

V. CONCLUSION

The basis of our investigations are the simulated spectra of three selected ionic liquids, $\text{EMIM}^+\text{BF}_4^-$, $\text{EMIM}^+\text{TfO}^-$ and $\text{BMIM}^+\text{BF}_4^-$, differing in the relative weighting of translation (dielectric conductivity) and rotation (dielectric permittivity). As we used a polarizable force field, the behaviour at optical frequencies could be extrapolated. The simulated spectra were converted to the solvation response function $S(t)$ within the framework of the reaction field continuum model. While experiments cannot separate the contributions from translation and rotation, simulated spectra allow for a detailed analysis in this regard.

Our findings can be summarized as follows. If one would use the dielectric spectra in the usual way, i.e. without the conductivity hyperbola, the formalism of the RFCM diverges, which was shown in particular for the mean relaxation time. Therefore, inclusion of the static conductivity is essential. Taken alone, it would give a

mono-exponential solvation response function. Proceeding from the static to the frequency-dependent conductivity already gives a qualitatively correct shape of $S(t)$. Taking the whole $\Sigma(\omega)$, which also includes rotation, only marginally changes the shape of the function. This shows very clearly the dominant role of the conductivity, i.e. of translational motion, a feature already encountered in previous studies.^{6,7,10,32,34}

In accordance with experimental studies,^{6-9,32} our simulations confirm that the RFCM predicts a too fast decay of $S(t)$ at longer times. We found that this can be traced back to a fundamental property of the dielectric behaviour of conducting systems. In the low-frequency region of the imaginary part of $\Sigma(\omega)$ the conductivity hyperbola $4\pi i\sigma_0/\omega$ suppresses the fine structure of all other contributions represented by $\Sigma_0(\omega)$. Generally, we used a fit function comprised of a mono-exponential describing the short-time regime and a KWW function representing the long-time behaviour. The inverse $1/\tau_2$ of the KWW relaxation time marks the onset of the region of divergence between $\Sigma(\omega)$ and $\Sigma_0(\omega)$.

For non-polarizable systems, where $\epsilon_\infty = 1$, the mean relaxation time of $S(t)$ is the very same, irrespective of the level of complexity, $4\pi i\sigma_0/\omega$, $4\pi i\sigma(\omega)/\omega$ or $\Sigma(\omega)$. It is exclusively determined by the inverse of σ_0 as well as by the value of the cavity dielectric constant ϵ_c . Adapting these parameters, the resulting $S(t)$ can be improved not only in its integral properties, but also in its functional shape. However, this remedy is only partially successful and depends on the system under consideration. We suggest that the extent of improvement depends on the size of that portion of the imaginary part of $\Sigma_0(\omega)$ that is suppressed by the conductivity hyperbola. In fact, for EMIM⁺TfO⁻ the deviations are the largest.

In the RFCM all parameters except for ϵ_c characterizing the solute cancel out upon normalization. We have tried to introduce more solute-specific features by considering the anisotropy of the solute in shape and charge distribution. The spherical cavity was replaced by an ellipsoid and the dipole moment was augmented by the quadrupole moment. However, within the RFCM anisotropic features of the solute do not create substantial changes in $S(t)$.

ACKNOWLEDGMENT

Although the experimental data of M. Maroncelli and N.P. Ernsting have been published meanwhile,⁷ we still gratefully acknowledge to have had them at hand prior to publication. We would like to thank the Vienna Scientific Cluster (<http://www.zid.tuwien.ac.at/vsc>) for the generous allocation of computer time. We are also grateful to the Austrian Science Fund FWF for funding this work in the context of Project No. P23494.

¹C. Schröder, C. Wakai, H. Weingärtner, and O. Steinhauser, J. Chem. Phys. **126**, 084511 (2007).

- ²C. Schröder, J. Hunger, A. Stoppa, R. Buchner, and O. Steinhauser, J. Chem. Phys. **129**, 184501 (2008).
- ³C. Schröder and O. Steinhauser, J. Chem. Phys. **132**, 244109 (2010).
- ⁴M. L. Horng, J. A. Gardecki, A. Papazan, and M. Maroncelli, J. Phys. Chem. **99**, 17311 (1995).
- ⁵X. Song, J. Chem. Phys. **131**, 044503 (2009).
- ⁶X.-X. Zhang, M. Liang, N. P. Ernsting, and M. Maroncelli, J. Phys. Chem. Lett. **4**, 1205 (2013).
- ⁷X.-X. Zhang, M. Liang, N. P. Ernsting, and M. Maroncelli, J. Phys. Chem. B **117**, 4291 (2013).
- ⁸X.-X. Zhang, M. Liang, J. Hunger, R. Buchner, and M. Maroncelli, J. Phys. Chem. B **117**, 15356 (2013).
- ⁹M. Liang, X.-X. Zhang, A. Kaintz, N. P. Ernsting, and M. Maroncelli, J. Phys. Chem. B **118**, 1340 (2014).
- ¹⁰M. Schmollngruber, C. Schröder, and O. Steinhauser, J. Chem. Phys. **138**, 204504 (2013).
- ¹¹B. M. Ladanyi and M. Maroncelli, J. Chem. Phys. **109**, 3204 (1998).
- ¹²B. M. Ladanyi and R. M. Stratt, J. Phys. Chem. **99**, 2502 (1995).
- ¹³R. M. Stratt and M. Cho, J. Chem. Phys. **100**, 6700 (1994).
- ¹⁴B. M. Ladanyi and R. M. Stratt, J. Phys. Chem. **100**, 1266 (1996).
- ¹⁵M. Maroncelli and G. R. Fleming, J. Chem. Phys. **89**, 5044 (1988).
- ¹⁶L. R. Martins, A. Tamashiro, D. Laria, and M. S. Skaf, J. Chem. Phys. **118**, 5955 (2003).
- ¹⁷P. V. Kumar and M. Maroncelli, J. Chem. Phys. **103**, 3038 (1995).
- ¹⁸N. Ito, S. Arzhantsev, and M. Maroncelli, Chem. Phys. Lett. **396**, 83 (2004).
- ¹⁹P. K. Chowdhury, M. Halder, L. Sanders, T. Calhoun, J. L. Anderson, D. W. Armstrong, X. Song, and J. W. Petrich, J. Phys. Chem. B **108**, 10245 (2004).
- ²⁰L. S. Headley, P. Mukherjee, J. L. Anderson, R. Ding, M. Halder, D. W. Armstrong, X. Song, and J. W. Petrich, J. Phys. Chem. A **110**, 9549 (2006).
- ²¹M. Maroncelli, X.-X. Zhang, M. Liang, D. Roy, and N. P. Ernsting, Faraday Discuss. **154**, 409 (2012).
- ²²B. L. Bhargava and S. Balasubramanian, J. Chem. Phys. **123**, 144505 (2005).
- ²³M. N. Kobrak, J. Chem. Phys. **125**, 064502 (2006).
- ²⁴Y. Shim, M. Y. Choi, and H. J. Kim, J. Chem. Phys. **122**, 044511 (2005).
- ²⁵Y. Shim, J. Duan, M. Y. Choi, and H. J. Kim, J. Chem. Phys. **119**, 6411 (2003).
- ²⁶D. Jeong, Y. Shim, M. Y. Choi, and H. J. Kim, J. Phys. Chem. B **111**, 4920 (2007).
- ²⁷M. N. Kobrak and V. Znamenskiy, Chem. Phys. Lett. **395**, 127 (2004).
- ²⁸H. K. Kashyap and R. Biswas, J. Phys. Chem. B **114**, 254 (2010).
- ²⁹S. Daschakraborty and R. Biswas, J. Chem. Phys. **137**, 114501 (2012).
- ³⁰S. Daschakraborty and R. Biswas, J. Phys. Chem. B **115**, 4011 (2011).
- ³¹S. Daschakraborty and R. Biswas, J. Chem. Phys. **139**, 164503 (2013).
- ³²X.-X. Zhang, C. Schröder, and N. P. Ernsting, J. Chem. Phys. **138**, 111102 (2013).
- ³³Y. Shim and H. J. Kim, J. Phys. Chem. B **117**, 11743 (2013).
- ³⁴Z. L. Terranova and S. A. Corcelli, J. Phys. Chem. B **117**, 15659 (2013).
- ³⁵S. Arzhantsev, H. Jin, G. A. Baker, and M. Maroncelli, J. Phys. Chem. B **111**, 4978 (2007).
- ³⁶C. J. F. Böttcher and P. Bordewijk, *Theory of electric polarization*, Vol. 2 (Elsevier, Amsterdam, 1978).
- ³⁷M. Maroncelli and G. R. Fleming, J. Chem. Phys. **86**, 6221 (1987).
- ³⁸Y. Mazurenko, Opt. Spectrosc. (USSR) **36**, 283 (1974).

- ³⁹C.-P. Hsu, X. Song, and R. A. Marcus, *J. Phys. Chem. B* **101**, 2546 (1997).
- ⁴⁰I. Rips, J. Klafter, and J. Jortner, *J. Chem. Phys.* **88**, 3246 (1988).
- ⁴¹T. G. Scholte, *Physica* **15**, 437 (1949).
- ⁴²C. J. F. Böttcher and P. Bordewijk, *Theory of electric polarization*, Vol. 1 (Elsevier, Amsterdam, 1978).
- ⁴³E. Castner, G. Fleming, and B. Bagchi, *Chem. Phys. Lett.* **143**, 270 (1988).
- ⁴⁴T. Darden, D. York, and L. Pedersen, *J. Chem. Phys.* **98**, 10089 (1993).
- ⁴⁵U. Essmann, L. Perera, M. L. Berkowitz, T. Darden, H. Lee, and L. G. Pedersen, *J. Chem. Phys.* **103**, 8577 (1995).
- ⁴⁶J.-P. Ryckaert, G. Ciccotti, and H. J. C. Berendsen, *J. Comput. Phys.* **23**, 327 (1977).
- ⁴⁷C. Schröder and O. Steinhauser, *J. Chem. Phys.* **133**, 154511 (2010).
- ⁴⁸B. R. Brooks, C. L. Brooks III, A. D. MacKerell Jr., L. Nilsson, R. J. Petrella, B. Roux, Y. Won, G. Archontis, C. Bartels, S. Boresch, A. Caffisch, L. Caves, Q. Cui, A. R. Dinner, M. Feig, S. Fischer, J. Gao, M. Hodoscek, W. Im, K. Kuczera, T. Lazaridis, J. Ma, V. Ovchinnikov, E. Paci, R. W. Pastor, C. B. Post, J. Z. Pu, M. Schaefer, B. Tidor, R. M. Venable, H. L. Woodcock, X. Wu, W. Yang, D. M. York, and M. Karplus, *J. Comput. Chem.* **30**, 1545 (2009).
- ⁴⁹C. Schröder, *J. Chem. Phys.* **135**, 024502 (2011).
- ⁵⁰A. Savitzky and M. J. E. Golay, *Anal. Chem.* **36**, 1627 (1964).
- ⁵¹K. Bica, M. Deetlefs, C. Schröder, and K. R. Seddon, *Phys. Chem. Chem. Phys.* **15**, 2703 (2013).